Inorganic Chemistry

pubs.acs.org/IC Article

Amino-Functionalized Mesoporous Silica Nanoparticle-Encapsulated Octahedral Organoruthenium Complex as an Efficient Platform for Combatting Cancer

Marina Martínez-Carmona,* Qui P. Ho, Jérémy Morand, Ana García, Enrique Ortega, Luiza C. S. Erthal, Eduardo Ruiz-Hernandez, M. Dolores Santana, José Ruiz,* Maria Vallet-Regí,* and Yurii Gun'ko

Cite This: https://dx.doi.org/10.1021/acs.inorgchem.0c01436 Read Online

ACCESS | Metrics & More | Article Recommendations | Supporting Information

ABSTRACT: In the process of synthesis of a new drug, as important as the drug itself is the formulation used, because the same compound can present a very different efficacy depending on how it is administered. In this work, we demonstrate how the antitumor capacity of a new octahedral organoruthenium complex, $[Ru(ppy\text{-}CHO)(phen)_2][PF_6]$ is affected by its encapsulation in different types of mesoporous silica nanoparticles. The interactions between the Ru complex and the silica matrix and how these interactions are affected at two different pHs (7.4 and 5.4, mimicking physiological and endolysosomal acidic conditions, respectively) have been studied. The encapsulation has also been shown to affect the induction of apoptosis and necrosis and progression of the cell cycle compared to the free drug. The encapsulation of the Ru complex in nanoparticles functionalized with amino groups produced very high anticancer activity in cancer cells *in vitro*, especially against U87 glioblastoma cells, favoring cellular internalization and significantly increasing the anticancer capacity of the initial non-encapsulated Ru complex.

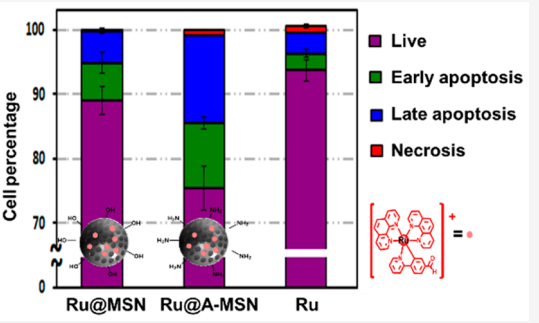

INTRODUCTION

The global phenomenon of cancer is an ever-growing social and economic burden and remains a major challenge in modern medicine.[1] Glioblastoma is one of the most aggressive and highly invasive malignant tumors that accounts for approximately half of adult brain tumors and is associated with poor prognosis and overall short survival.[2] A majority of glioblastoma tumors are not amenable to surgery as these neoplastic cells invade surrounding brain tissue, rendering complete resection difficult.[3] In addition, most cases of ovarian epithelial carcinoma, which is a leading cause of cancer death in women, are associated with poor prognosis and low survival rates.[4] Hence, there is an urgent need for novel chemotherapeutic formulations for these types of cancer.

The formulation of novel drugs using delivery systems is essential to optimize their therapeutic performance. The way in which a compound enters the body, reaches its place of action, and interacts with the target tissues and cells can be modulated by nanocarriers, which plays a key role in reaching the desired effectiveness.[5] By tuning the properties of the nanocarrier, the delivery process can be adapted to the specific drug, which is especially important when the compounds are insoluble or cytotoxic, thus presenting a reduced activity or severe side effects before reaching their target. Due to their unique and versatile biochemical properties, ruthenium-based compounds have emerged as very promising anticancer agents that can serve as alternatives to cisplatin and its derivatives.[6−10] For example, the ruthenium(III) complex NKP-1339 is undergoing clinical trials for cancer treatment,[11] and $Ru^{II}(\eta^6\text{-arene})$ complexes have been investigated for their tunability and novel modes of action.[12−15] The combination of polypyridyl ruthenium drugs with nanoscale drug delivery systems has garnered a great deal of research attention.[16,17] Compared with the planar structure of platinum drugs, the octahedral configuration of ruthenium complexes provides a rigid framework for the construction of a nanocarrier and their planar ligands may provide hydrophobic cavities for drug loading.[18] However, many Ru complexes have limited capacity to cross the cell membrane.[19,20]

Mesoporous silica nanoparticles (MSNs) have unique properties such as a large surface area, high stability and degree of tunability, and good biocompatibility, making them excellent vehicles for the delivery of any type of drug, especially one with antitumor purposes.[21] Other materials widely used in drug delivery are liposomes and polymeric nanoparticles. Unlike the first ones with low stability or the second ones

Received: May 15, 2020

https://dx.doi.org/10.1021/acs.inorgchem.0c01436
Inorg. Chem. XXXX, XXX, XXX−XXX

whose release kinetics are very fast, MSNs are resistant and allow sustained release over time.[22] Thus, MSNs are potentially among the best nanocarriers for solving drug delivery problems.[21,23,24] Dysfunctional vascular architecture represents a common feature of the tumor microenvironment that presents a suitable situation for nanometric agents to pass through efficiently because of the enhanced permeability and retention (EPR) effect.[25] Furthermore, the use of stimulus-response nanoparticles favors drug release in a controlled manner, following the accumulation in the tumor environment and only after the desired stimulus. Said stimulus may come from an external source (light, magnetic field, ultrasound, etc.) or be defined by internal tumor conditions (redox, pH, etc.).[26] The tumor microenvironment is known to be acidic due to high cellular metabolic rates. This variation in pH has previously been reported as strategy to uncap the silica pores[27,28] or to weaken drug−matrix interactions,[29,30] in each case triggering the release of the loaded molecules.

Despite that, so far only a few systems have combined MSNs with Ru complexes, mainly for imaging applications.[31,32] Frasconi et al. reported MSNs with kinetically inert ruthenium-(II) polypyridyl complexes grafted on the surface,[33] and Lv et al. designed chitosan MSNs for the delivery of a ruthenium(II) N-heterocyclic carbene (RuNHC) complex.[34]

However, to the best of our knowledge, no studies about how different formulations affect the antitumor efficacy of a Ru complex have been performed. In addition, it is necessary to take into account how pH affects the different MSN−Ru complex interactions when modifying the chemical nature of the mesoporous matrix

Moreover, it has been recently shown that a class of kinetically inert cyclometalated Ru(II) complexes of the type $[Ru(C^N)(N^N)_2]^+$ exhibits selective cytotoxicity in cancer cells through a distinct mode of action that involves proteosynthesis inhibition rather than targeting nuclear macromolecules like DNA like other conventional metal-based agents.[35]

Herein, we report our studies and comparison of the *in vitro* anticancer activity of the octahedral cationic C,N-cyclometalated Ru(II) anticancer agent (Figure 1) $[Ru(ppy-CHO)(phen)_2]^+$ [ppy-CHO = deprotonated 4-(pyridin-2-yl)benzaldehyde][35] when administered free or loaded into mesoporous silica nanoparticles. Special attention is also paid to understand the consequences of using the nanoparticles as drug transporters at the cellular level, its pH-dependent cargo release and cancer cell internalization, and the mode of cell death induced upon treatment.

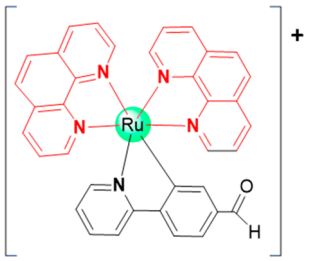

Figure 1. Structure of the $[Ru(ppy-CHO)(phen)_2]^+$ [C^N = deprotonated 4-(pyridin-2-yl)benzaldehyde] complex.

RESULTS AND DISCUSSION

Preparation and Characterization of the Nanosystems. In this work, two different types of MSN have been synthesized: (i) bare ones, with silanol groups on the surface and negative ζ potentials, denoted as MSNs, and (ii) A-MSN, obtained by co-condensation between tetraethyl orthosilicate (TEOS) and (3-aminopropyl)triethoxysilane (APTES), which present amino groups and have positive ζ potentials. Scanning electron microscopy (SEM) images (Figure 2) show that in both cases we have discrete particles of ∼200 nm for MSN and ∼150 nm for A-MSN. A complete characterization study shows that both nanoparticle types present similar pore arrangements and textural properties.

The presence of amino groups was confirmed by Fourier transform infrared spectroscopy (FTIR). Figure S1A displays spectra of mesoporous silica nanoparticles with and without amine groups. The A-MSN sample shows the appearance of a new band at ∼1590 cm^{-1} corresponding to the bending vibration mode of N−H due to functionalization with $-NH_2$ groups. With regard to the structural characterization of MSN and A-MSN samples before ruthenium loading, powder X-ray diffraction (XRD) confirms the two-dimensional hexagonal mesoporous arrangement, displaying three well-defined reflections that can be indexed as 10, 11, and 20 of a *p6mm* space group for both materials. Additionally, the MSN shows an extra reflection index as 21 (Figure S1B).

The porosities of MSN and A-MSN materials have been characterized by N_2 adsorption/desorption analyses, and the main parameters are listed in Table S1. Panels C and D of Figure S1 show the N_2 adsorption isotherms and mesopore size distributions, respectively. Isotherms are type IV according to the IUPAC classification, which are characteristic of mesoporous materials exhibiting parallel cylindrical pores.[36]

Both the surface area (S_{BET}) and the pore diameter (D_P) decrease slightly when the amine groups are introduced by co-condensation compared to pure silica nanoparticles. These findings are in accordance with the calculated wall thickness (t_{wall}) values, which increase slightly when the walls are functionalized with amino groups. To acquire information regarding the mean size and surface charge of the nanosystems, dynamic light scattering (DLS) and ζ potential measurements were recorded. DLS measurements show good dispersions with a narrow size distribution in water for both types of nanoparticles (Figure S2). The mean hydrodynamic sizes determined by DLS were found to be 220 nm for MSN and 180 nm for A-MSN, which, as expected, are slightly larger than those estimated from SEM images. ζ potential measurements recorded at two different pHs (7.4 and 5.4, mimicking physiological and endolysosomal acidic conditions, respectively) showed notable variations in the superficial charge of the nanoparticles (Table 1). Ru complex loading was carried out by the impregnation method in a dimethylformamide (DMF) solvent, and the amount of drug loaded was calculated by subtracting the data obtained by thermogravimetric analysis (TG) for the loaded and unloaded samples. The percentage weight reduction includes evaporation of water (0−100 °C), degradation of most of he organic material (100−300 °C), and dehydration of the particle's silanol groups starting at 300 °C. Therefore, only the difference in percentage weight reduction within the range of 100−300 °C (range in which the Ru complex is removed) was taken into account to calculate the amount of the loaded drug (Figure S3). The values obtained

https://dx.doi.org/10.1021/acs.inorgchem.0c01436
Inorg. Chem. XXXX, XXX, XXX−XXX

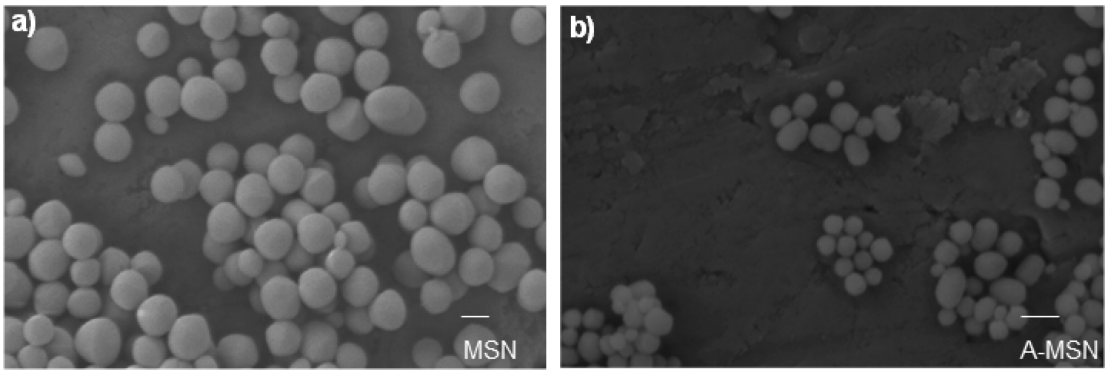

Figure 2. SEM images of (a) MSN and (b) A-MSN. Scale bars, 200 nm.

Table 1. ζ Potentials (millivolts) of MSN and A-MSN at Two Different pHs

	pH 5.4	pH 7.4
MSN	−3.98 ± 0.36	−17.21 ± 0.74
A-MSN	21.30 ± 0.53	9.37 ± 0.39

showed that both materials had a comparable loading capacity with percentages of 1.47% and 2.12% (w/w) for MSN and A-MSN, respectively.

The comparison of TEM images before and after loading for A-MSN, as an example (Figure 3), demonstrates that the presence of the Ru complex inside the pores of the nanoparticles does not modify the morphology of the nanoparticles. Additionally, the presence of Ru was evaluated using FTIR of the loaded samples (Figure S4) and energy dispersive X-ray analysis (EDX). TEM−EDX and SEM−EDX analysis (Figure S5) confirmed the presence of ruthenium loaded inside the mesopores of nanoparticles. Ru was detected by TEM−EDX analysis in the Ru@A-MSN sample but not in Ru@MSN. The Ru@MSN sample loaded a smaller amount of Ru compared to the amino-functionalized nanosystem, and although the difference between both is very small, it coincides with the detection limits of the TEM−EDX technique, which makes it impossible to detect Ru in the Ru@MSN sample. On the other hand, SEM−EDX analysis confirmed the presence of Ru in both samples (Figure S5B).

"In Vial" Cargo Release Experiments. To ensure that the integrity of the drug was not affected by the encapsulation process, the absorption spectrum of the complex was measured before loading and after being released by both types of nanoparticles. No differences were observed in any of the cases (Figure S6). Additionally, the stability of the complex after being released was also confirmed by mass spectrometry (Figures S7 and S8).

Although the surface functionalization does not seem to significantly affect the morphological, structural, or textural properties of the particles, their important differences in ζ potentials (Table 1) have a considerable influence on the release profile of the complex.

Ru release profiles for both Ru@MSN and Ru@A-MSN were obtained at two different pHs (7.4 and 5.4, mimicking physiological and endolysosomal acidic conditions, respectively). The Ru concentration after different assay times was quantified by absorption measurements (λ = 510 nm). As shown in Figure 4, the release profile of Ru@A-MSN, with a ζ potential of 21.30 mV at pH 5.4, presents a very sharp initial burst and a release of practically 100% 72 h after the beginning of the experiment. This fast and extensive release is probably facilitated by repulsion forces between the positive charges of the Ru complex and the amino groups.

In contrast, the profile of A-MSN at physiological pH, where the ζ potential is reduced to 9.37 mV and repulsion forces decrease, displays a slower and sustained release over time. MSN at pH 5.4 presents a ζ potential of −3.98 mV, closer to that of A-MSN at pH 7.4, which is consistent with the fact that they present similar release profiles. However, at pH 7.4, its ζ potential becomes more negative (−17.21 mV), favoring the

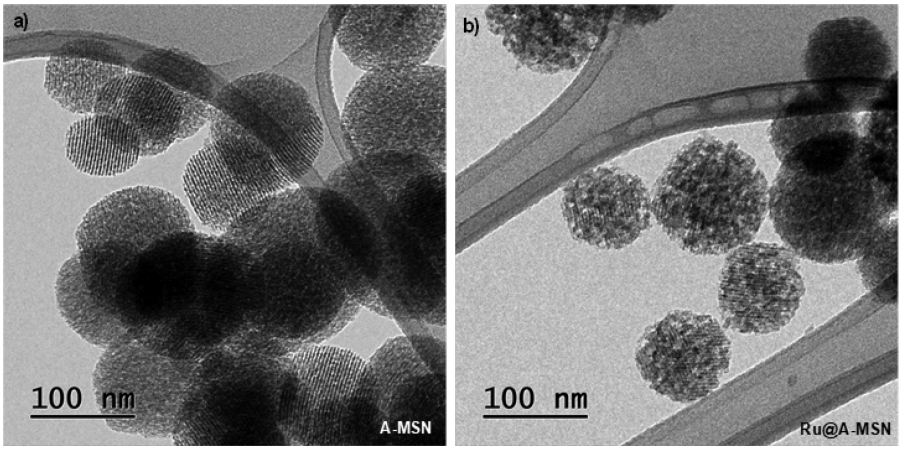

Figure 3. TEM images of (a) A-MSN and (b) Ru@A-MSN.

https://dx.doi.org/10.1021/acs.inorgchem.0c01436
Inorg. Chem. XXXX, XXX, XXX−XXX

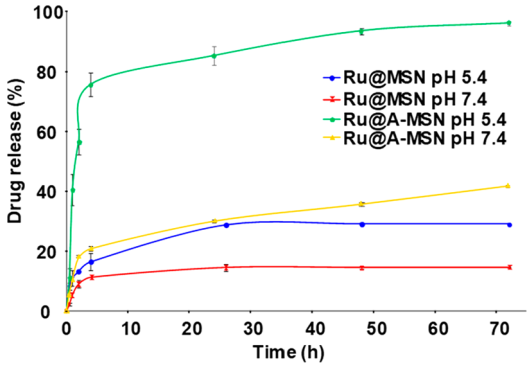

Figure 4. "In vial" cumulative Ru complex release profiles for Ru@MSN and Ru@A-MSN nanosystems at two different pHs (5.4 and 7.4).

interactions with the Ru complex and therefore giving rise to a minor release of approximately 10% of the loading 72 h after the start of the experiment.

Release profiles can be adjusted to a first-order kinetic model by introducing an empirical non-ideality factor (δ) to give the following (eq 1):[37]

$$Y = A(1 - e^{-kt})^{\delta} \quad (1)$$

where Y is the percentage of $[Ru(ppy\text{-}CHO)(phen)_2]^+$ released at time t, A the maximum amount of Ru complex released (in percentage), and k the release rate constant. The values for δ are between 1 for materials that obey first-order kinetics and 0 for materials that release the loaded cargo at the very initial time of the test. The parameters of the kinetic fitting shown in Figure S9 indicate that at pH 5.4 A-MSN presents a kinetic of order of 0, releasing the cargo in a short period of time probably due to the repulsion forces. The obtained δ and k values for A-MSN at pH 7.4 and MSN at pH 5.4 are very similar, pointing to similar drug−matrix interactions. Finally, the δ value for MSN at pH 7.4 is almost 1, pointing to a near first-order kinetics with a slight contribution of an initial burst release of the loaded molecules.

***In Vitro* Biological Evaluation.** Once both samples were deeply characterized and their release response was tested "in vial", we proceeded to investigate their *in vitro* performance as drug delivery nanocarriers.

The *in vitro* cytotoxicity of the drug-loaded nanoparticles and their potential application in cancer treatment were evaluated in cell culture models. The antiproliferative activities of the nanoparticles were evaluated in U87 glioblastoma cells, A2780 ovarian cancer cells, and CHO normal cells. After being incubated for 2 h and cultured for 72 h, the nanoparticles showed cytotoxicity in a dose-dependent manner in all tested cell lines (Figure 5).

It is worth noting that both Ru@MSN and Ru@A-MSN proved to be markedly less cytotoxic to normal ovarian cells, suggesting differential selectivity toward cancer cells. Specifically, Ru@A-MSN produced a reduction in cell viability 2 times greater in U87 cells than in CHO cells for all concentrations and ≤4 times greater in A2780 cells for the maximum concentration. Compared to Ru@A-MSN, Ru@MSN did cause a smaller decrease in cell viability, indicating that the A-MSN nanocarrier might be suitable for use with small metal complexes with anticancer activity. Although Ru@A-MSN turned out to be more effective in both tumor cells, a more pronounced difference in cytotoxicity in U87 cells, coupled with the challenge of trying to treat a tumor as aggressive as glioblastoma, motivated the investigation to focus on this cell type.

Therefore, a detailed cytotoxicity study of the loaded nanoparticles was carried out and compared with the effect caused by the empty nanoparticles and the equivalent amount of free Ru complex. U87 cells were incubated for 2 h with different concentrations (25, 50, and 100 μg/mL) of loaded or unloaded nanomaterials and analyzed 24 or 72 h later. Taking into account the loading capacity of Ru@A-MSN (2.12%), we added equivalent free Ru complex concentrations (approximately 0.5, 1, and 2 μg/mL, respectively) as a control. The results in Figure 6 demonstrate that after 72 h, none of the unloaded nanoparticles were cytotoxic (viability of >90%) at concentrations of ≤100 μg/mL. Figure 6a shows that 24 h after the treatment, Ru@MSN did not produce significant death and free Ru reduced cell viability by only 10% at the maximum concentration tested. However, Ru@A-MSN managed to reduce cell viability by half at a Ru concentration of 1 μg/mL.

Remarkably, an 8-fold concentration of free Ru was necessary to achieve the same effect (Figure S10). After 72 h, Ru@MSN was able to reduce cell viability to 72%, and although in the presence of free Ru the viability was severely reduced to 31%, Ru@A-MSN was demonstrated to be the most effective treatment, reducing cellular viability to 15% in a dose-dependent manner. These results are consistent with the release profiles obtained for both types of particles. The maximum release of Ru@MSN up to 72 h is only around 20% of the total loading, which explains that at 24 h practically no cytotoxic effects are observed and after 72 h cell viability is just slightly reduced. In contrast, Ru@A-MSN had a large initial burst capable of producing a significant decrease in cell viability, and it eventually released almost 100% of the loading after 72 h, when most of the cancer cells have been killed.

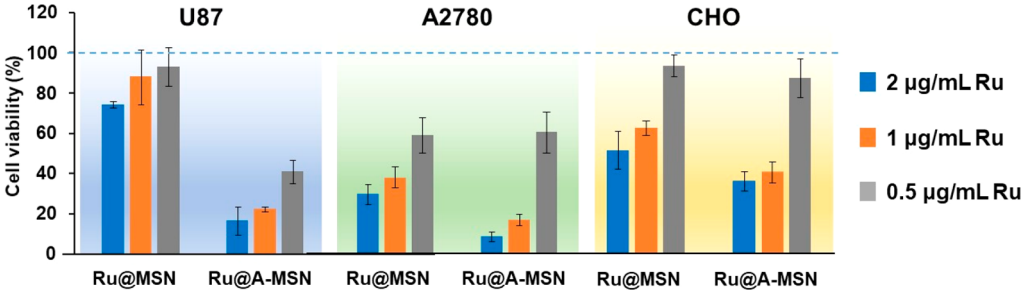

Figure 5. Cytotoxicity of U87 glioblastoma cells, A2780 cancer cells, and CHO normal cells after treatment for 72 h with increasing concentrations of Ru@MSN or Ru@A-MSN. The concentration is expressed as a function of the loaded Ru, and the blue dotted line indicates the control.

https://dx.doi.org/10.1021/acs.inorgchem.0c01436
Inorg. Chem. XXXX, XXX, XXX−XXX

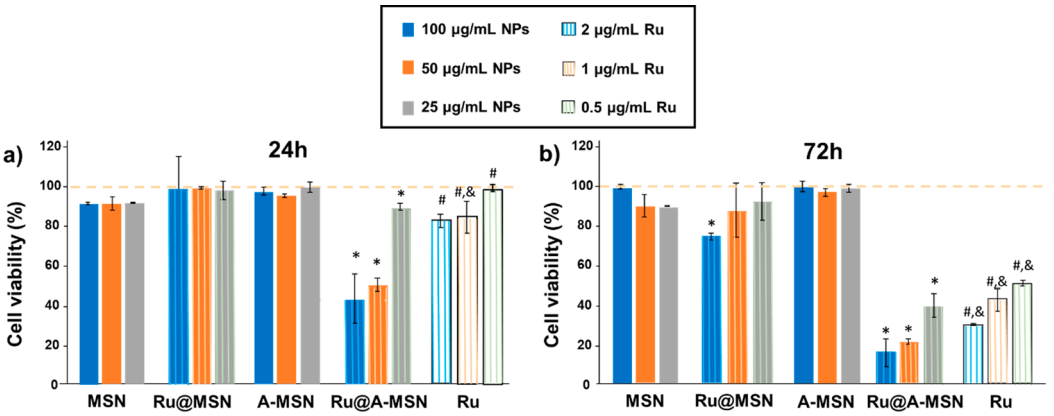

Figure 6. Viability of U87 glioblastoma cells after treatment for 2 h with different concentrations of MSM, A-MSN, Ru@MSN, Ru@A-MSN, and the equivalent free Ru complex and posterior culture for (a) 24 h or (b) 72 h, measured by Cell Counting Kit-8 (CCK-8). Statistical significance was calculated using an unpaired *t* test. $^{*}p < 0.05$ comparing loaded with unloaded nanoparticles. $^{\#}p < 0.05$ comparing Ru@A-MSN with the equivalent free Ru complex. $p < 0.05$ comparing Ru@MSN with the equivalent free Ru complex.

The presence of amino groups on the surface of MSNs was expected to improve the internalization of the cationic Ru complex in cancer cells due to stronger interactions between the positive A-MSN and the negatively charged phospholipids of the cell membrane.[38,39] To test that effect, U87 human glioblastoma cells were incubated in the presence of size and ζ potential value comparable fluorescein-labeled MSNs (see Experimental Section for preparation and Figure S11 for characterization). As one can see in Figure 7, representative confocal microscopy images revealed a larger amount of A-MSN inside U87 tumor cells after incubation for 2 h as compared to the amount of MSN, which showed negligible internalization.

However, these differences in internalization seem to decrease over time because when the incubation with the loaded nanoparticles is carried out for a longer period of time (24 h), the content of metal inside U87 cells, evaluated by inductively coupled plasma mass spectrometry (ICP-MS), showed that although the level of Ru was higher in cells treated with Ru@A-MSN, Ru@MSN also led to important amounts of Ru (Figure S12). What is more interesting is that treatment with either type of nanoparticle resulted in a content of ruthenium that was higher than that of the free equitoxic complex. The results support the proposal of using nanoparticles for drug administration.

To better understand the effect of the encapsulation on antitumor capacity, cell cycle progression studies and apoptosis/necrosis induction studies were performed. The progression of the cell cycle analysis shows that compared to untreated U87 cells, treatment with Ru@A-MSN nanoparticles produced cell death and increased the S phase cell population slightly. However, Ru@MSN treatment resulted in an increase in the G1 phase cell population with a concomitant reduction in the S phase cell population. Moreover, treatment with an equivalent quantity of the free ruthenium complex did not yield these minor cell cycle perturbations (Figure 8). In contrast, the well-known DNA damage agent cisplatin slightly induced S and G2/M phase arrest.[40] Although these alterations in cell cycle distribution were not significantly different from untreated cells, the induced changes observed might be due to the unique mechanism of action of the loaded Ru complex in cancer, which involves the inhibition of proteosynthesis,[33] a process that occurs in the G1 phase.

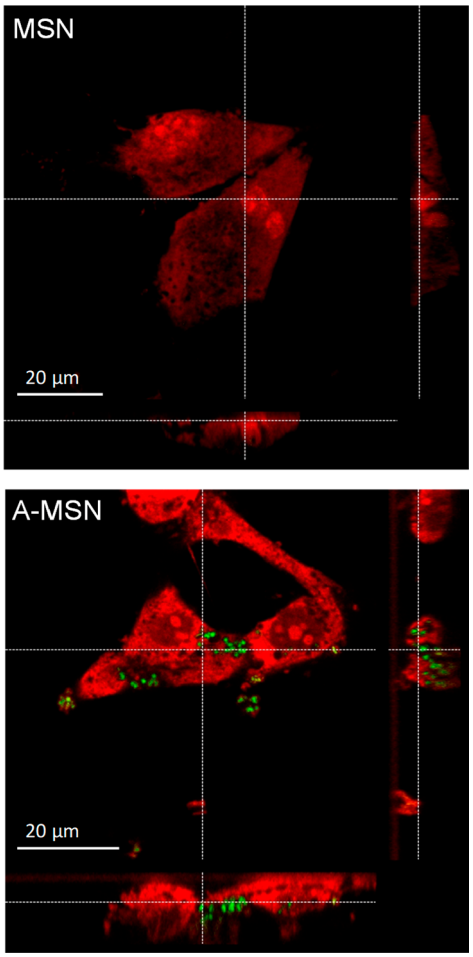

Figure 7. Internalization study by confocal microscopy of 50 μg/mL green-labeled nanopaticles after incubation for 2 h. The bottom and side panels show the *x*−*z* and *y*−*z* cross-sectional images, respectively.

The cell death induction treatments in U87 were evaluated after 24 h using dual Annexin V/propidium iodide (PI) staining. The flow cytometric assay allowed the detection of necrotic cell populations (Annexin V−/PI+ quadrant) and both early and late apoptotic cells (Annexin V+ quadrants). Treatments with both Ru@MSN and Ru@A-MSN nanoparticles revealed apoptotic induction as indicated by Annexin

https://dx.doi.org/10.1021/acs.inorgchem.0c01436
Inorg. Chem. XXXX, XXX, XXX−XXX

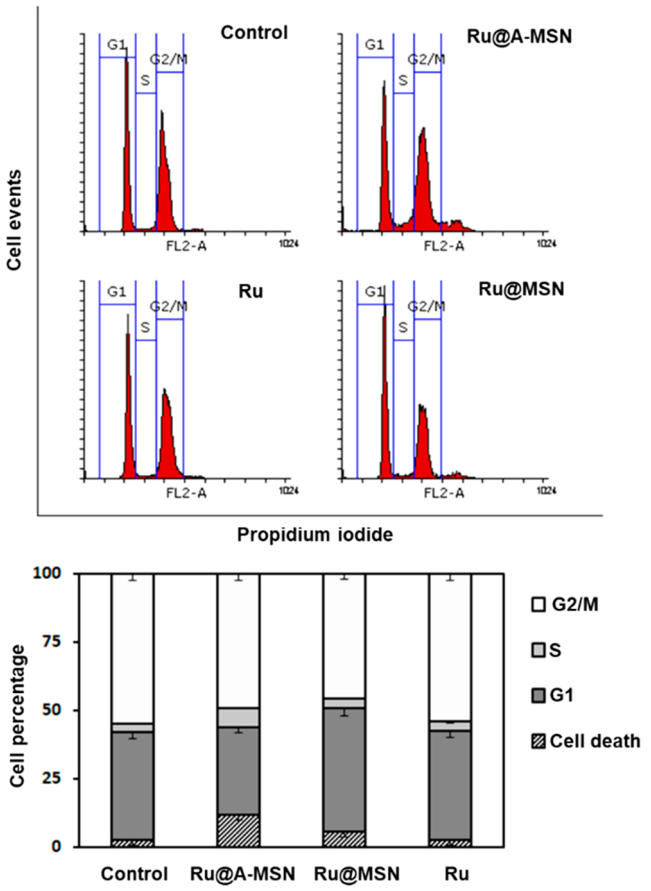

Figure 8. Cell cycle analysis of U87 cells after treatment with Ru-loaded nanoparticles (150 μg/mL) or equivalent free ruthenium complex (3 μg/mL) for 3 h, determined by propidium iodide intensity by flow cytometry.

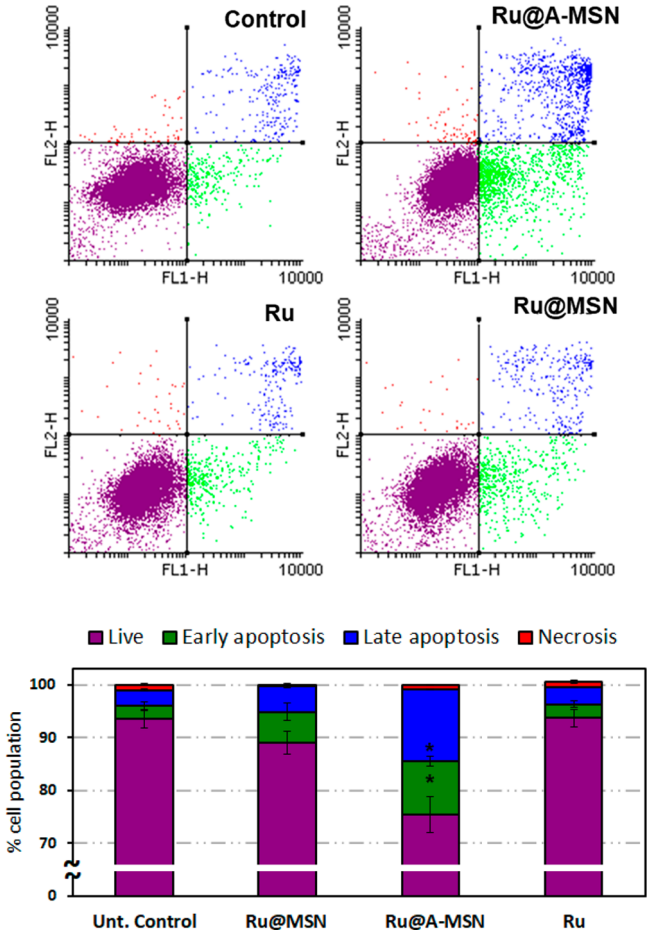

Figure 9. Dual Annexin V-FITC (FL1-H)/propidium iodide (FL2-H) flow cytometric analysis of U87 cells cultured for 24 h after treatment (3 h) with loaded nanoparticles (150 μg/mL) or the equivalent free ruthenium complex (3 μg/mL). Untreated cells were used as a control. Statistical significance was calculated using an unpaired t test (*$p < 0.05$) from two independent experiments ($n = 2$ replicates).

V-labeled cell populations; Ru@A-MSN produced a greater extent of apoptosis (Figure 9). However, the administration of the free ruthenium complex at equivalent concentrations in the nanoparticles has not resulted in apoptotic cell death. This clearly shows that delivery of the ruthenium complex using these nanocarriers improved the promotion of cell death by apoptosis in U87 cells.

CONCLUSIONS

In this work, a new nanodrug based on [Ru(ppy-CHO)-(phen)$_2$][PF$_6$]-loaded mesoporous silica nanoparticles has been developed. The effects of the formulation on the potential anticancer efficacy of the complex have been studied *in vitro* against glioblastoma and ovarian cancer cells, with particular focus on the interactions between the Ru complex and the silica matrix at two different pHs (7.4 and 5.4, mimicking physiological and endolysosomal acidic conditions, respectively). Ru@A-MSN has demonstrated the highest effectiveness against both tumor cell lines. For glioblastoma cells, cell viability decreased to <50% after treatment for 24 h for a concentration as low as 1 μg/mL, which is 8 times more efficient than the free Ru complex. In addition, compared to free equitoxic Ru complex treatment, administration of nanocarriers resulted in a higher level of accumulation of ruthenium within cancer cells; nanoparticles can slightly alter the cell cycle progression in glioblastoma cells, particularly in the G1 phase, and cause moderate apoptotic cell death induction after 24 h.

These outcomes demonstrate the importance of the formulation and nanosystems in the administration of a drug and open a new field of research that combines nanoparticles and Ru complexes for the treatment of cancer.

EXPERIMENTAL SECTION

Reagents. Tetraethylorthosilicate (TEOS, 98%), sodium hydroxide (NaOH, ≥98%), *n*-cetyltrimethylammonium bromide (CTAB, ≥99%), ammonium nitrate (NH_4NO_3, ≥98%), (3-aminopropyl)-triethoxysilane (APTES, ≥98%), 4-(pyridin-2-yl)benzaldehyde (pyba), potassium hexafluorophosphate, fluorescein 5(6)-isothiocyanate (FITC, ≥98%), and 1,10-phenanthroline (phen) were purchased from Sigma-Aldrich, and the ruthenium compound was purchased from Johnson Matthey. All chemicals were used as received without further purification.

Characterization Techniques. XRD experiments were performed in a Philips X'Pert diffractometer equipped with Cu Kα radiation (wavelength of 1.5406 Å) (Philips Electronics NV, Eindhoven, The Netherlands). XRD patterns were collected in the 2θ range of 0.6−8° with a step size of 0.02° and a counting time of 5 s per step. Thermogravimetric (TG) measurements were performed in a PerkinElmer Pyris Diamond TG/DTA instrument (heating from 25 to 100 °C at 10 °C/min, hold for 5 min at 100 °C to remove all

https://dx.doi.org/10.1021/acs.inorgchem.0c01436
Inorg. Chem. XXXX, XXX, XXX−XXX

remaining water, and heat from 100 to 900 °C). Fourier transform infrared spectroscopy (FTIR) was carried out in a Nicolet (Thermo Fisher Scientific, Waltham, MA) Nexus spectrometer equipped with a Goldengate attenuated total reflectance (ATR) accessory (Thermo Electron Scientific Instruments LLC, Madison, WI). The morphology, mesostructural order, and nanoparticle functionalization were studied by high-resolution transmission electron microscopy (HRTEM) with a JEOL JEM 3000F instrument operating at 300 kV, equipped with a CCD camera (JEOL Ltd., Tokyo, Japan). Sample preparation was performed by dispersing in EtOH and subsequent deposition onto carbon-coated copper grids. Energy dispersive X-ray analysis (EDX) was carried out in combination with SEM and TEM. For this purpose, TEM−EDX analyses were carried out with a JEOL JEM 1400 (JEOL Ltd.) instrument equipped with a CCD camera (KeenView Camera) and operated at 120 kV. SEM images were obtained with the Zeiss Ultra Plus scanning electron microscope. Samples were prepared by dispersion in ethanol and subsequent deposition onto a copper stud, dried, and coated with a film of gold prior to observation. SEM−EDX analysis was performed on a JEOL 6100 instrument operating at 20 kV. Samples were prepared by powder deposition onto a copper stud, dried, and coated with a film of gold prior to observation.

To determine the surface charge of nanoparticles by ζ potential measurements, a Zetasizer Nano ZS (Malvern Instruments) equipped with a 633 nm "red" laser was used. ζ potential measurements were recorded in aqueous colloidal suspensions at pH 5.4 and 7.4. For this purpose, 1 mg of nanoparticles was added to 10 mL of solvent followed by sonication for 5 min to obtain a homogeneous suspension. In both cases, measurements were recorded by placing 1 mL of the suspension (0.1 mg mL^{-1}) in DTS1070 disposable folded capillary cells (Malvern Instruments). The textural properties of the materials were determined by N_2 adsorption porosimetry by using a Micromeritics ASAP 2020 instrument (Micromeritics Co., Norcross, GA). To perform the N_2 measurements, 20−30 mg of each sample was previously degassed under vacuum for 24 h at 40 °C. The surface area (S_{BET}) was determined using the Brunauer−Emmett−Teller (BET) method, and the pore volume (V_P) was estimated from the amount of N_2 adsorbed at a relative pressure of ∼0.97. The pore size distribution between 0.5 and 40 nm was calculated from the adsorption branch of the isotherm by means of the Barrett−Joyner−Halenda (BJH) method. The mesopore size (D_P) was determined from the maximum of the pore size distribution curve. C, H, and N analyses were performed with a Carlo Erba model EA 1108 microanalyzer. The ^{1}H spectra were recorded on a Bruker AV 400 spectrometer. Chemical shifts are cited relative to the solvent resonance. ESI mass (positive mode) analyses were performed on a HPLC/MS TOF 6220 instrument.

Synthesis of Pure Silica (MSN) and Amino-Functionalized (A-MSN) Mesoporous Silica Nanoparticles. Bare MSNs, denoted as MSN, were synthesized by the modified Stöber method using TEOS as the silica source in the presence of CTAB as the structure-directing agent. Briefly, 1 g of CTAB, 480 mL of H_2O, and 3.5 mL of NaOH (2 M) were added to a 1 L round-bottom flask. The mixture was heated to 80 °C and magnetically stirred at 600 rpm. When the reaction mixture was stabilized at 80 °C, 5 mL of TEOS was added dropwise at a rate of 0.33 mL min^{-1}. The white suspension obtained was stirred for a further 2 h at 80 °C. The nanoparticles were collected by centrifugation, washed twice with water and twice with ethanol, and stored in an ethanol suspension.

A-MSN was synthesized in the same way but replacing 10% of TEOS with APTES.

Synthesis of Fluorescent Nanoparticles. For cellular internalization studies, fluorescein-labeled MSNs were synthesized. For this purpose, 1 mg of FITC and 2.2 μL of APTES were dissolved in 100 μL of ethanol and allowed to react for 2 h. Then the reaction mixture was added with TEOS or with TEOS and APTES as previously described.[41]

Synthesis of the Ru Complex (Ru). The ruthenium complex $[Ru(ppy\text{-}CHO)(phen)_2][PF_6]$ was prepared according to the literature procedure reported by us.[35]

Anal. Calcd for $C_{36}H_{24}F_6N_5OPRu$ (788.66): C, 54.83; H, 3.07; N, 8.88. Found: C, 54.72; H, 3.01; N, 8.93. ESI-MS (m/z): 644.1139 ($M - PF_6$)$^+$. ^{1}H NMR (400 MHz, CD_3CN, 25 °C): δ 9.59 (s, 1H), 8.50 (dd, 1H, J = 8.21, 1.36 Hz), 8.40 (multiplet, 4H), 8.22 (dd, 1H, J = 5.29, 1.20 Hz), 8.18 (d, 1H, J = 8.21 Hz), 8.16 (s, 2H), 8.12 (s, 2H), 8.09 (dd, 1H, J = 4.97, 1.36 Hz), 8.05 (d, 1H, J = 8.06 Hz), 7.90 (dd, 1H, J = 5.33, 1.20 Hz), 7.74 (td, 1H, J = 7.62, 1.54 Hz), 7.66 (dd, 1H, J = 5.66, 1.45 Hz), 7.63 (dd, 3H, J = 8.18, 5.21 Hz), 7.47 (dd, 1H, J = 8.14, 5.33 Hz), 7.36 (dd, 1H, J = 7.98, 1.72 Hz), 6.93 (td, 1H, J = 5.66, 1.45 Hz), 6.87 (d, 1H, J = 1.60 Hz).

Loading with the Ru Complex. Two samples of 20 mg of MSN and A-MSN were collected by centrifugation and suspended in 2 mL of a DMF/Ru complex solution (3 mg/mL) while being stirred for 24 h. Then, Ru@MSN and Ru@A-MSN samples were centrifuged and washed twice with water. After being washed, one sample of each type was dried under vacuum to carry out TG studies and the other was suspended in 800 μL of water for the release experiments.

"In Vial" Cargo Release Assays. The suspensions of the previous section were divided into four vials each with a volume of 200 μL; 800 μL of phosphate-buffered saline (PBS) with a pH 5.4 or 7.5 was used to obtain a final volume of 1 mL. The suspensions were sonicated for a few seconds, and then to avoid limitations of the delivery rate by external diffusion constraints, continuous stirring was maintained during the assays.

After determined periods of time, samples were centrifuged, the PBS was collected, and a fresh 1 mL portion of the corresponding PBS was added to continue the release. The cumulative Ru complex released was determined by absorption measurements (λ = 510 nm). The Ru complex concentration was determined from the average of the readings from four different samples (N = 4), and data are presented as the mean ± the standard deviation. The calibration curve was made at both pHs ensuring that this parameter would not influence the results.

Cell Culture. The U87 MG human glioblastoma cell line was cultured in Minimum Essential Medium Eagle (MEM) (Sigma-Aldrich) supplemented with 10% FBS and 1% L-glutamine. Human ovarian cancer cells (A2780) were cultured in Roswell Memorial Park Institute (RPMI)-1640 medium (Biowest) supplemented with 10% FBS and 2 mM L-glutamine. Normal ovarian cancer cells, CHO (Chinese hamster ovary), were cultured in F-12 medium supplemented with 10% FBS and 2 mM L-glutamine. The cell lines were maintained in a humidified atmosphere of 5% CO_2 at 37 °C with a subculture routine of two or three times per week at appropriate densities according to the cell line requirements.

Internalization Assays in U87 MG Cells. Experiments were conducted in μ-Slide 8 Well ibiTreat #1.5 polymer coverslips (tissue culture-treated, sterilized). For nanoparticle uptake, cells were incubated with medium containing nanoparticle suspensions (50 μg/mL) for 2 h. The chambers were thoroughly washed with PBS to remove the non-internalized particles. Then, cells were fixed with 4% paraformaldehyde for 20 min and washed twice with PBS. Then, cells were stained for 10 min by adding 200 μL of PBS and 1 μL of SYTO 60 Red Fluorescent Nucleic Acid Stain (Molecular Probes) per well and washed with PBS. The images were acquired using a Leica SP8 scanning confocal microscope (scanning confocal with lasers for 405, 488, 552, and 638 nm and 3PMT detectors). For the purpose of presentation, pictures were exported in JPG format.

Biocompatibility of MSN and A-MSN in U87 MG Cells. For the cell viability test, the cells were seeded on 24-well plates at an initial density of 25000 cells/well and left to attach for 24 h. The cells were treated with empty mesoporous silica nanoparticles at three different concentrations (25, 50, and 100 μg/mL). After the incubation period (24 or 72 h), cell viability was evaluated using Cell Counting Kit-8 (CCK-8) (Dojindo). The reagent was directly mixed with fresh medium and placed in contact with the cells for 1 h at 37 °C. Then, the absorbance at 450 nm was read. The viability was plotted as a percentage (%) of the absorbance normalized for the control.

Cytotoxicity of the Free Ru Complex against U87 MG Cells. The cells were treated with increasing concentrations of the Ru

https://dx.doi.org/10.1021/acs.inorgchem.0c01436
Inorg. Chem. XXXX, XXX, XXX−XXX

complex and incubated for 2 h. Then, the cell viability was evaluated (CCK-8). The reagent was directly mixed with fresh medium and placed in contact with the cells for 1 h at 37 °C. Then, the absorbance at 450 nm was read. The viability was plotted as a percentage (%) of the absorbance normalized for the controls.

Cytotoxicity of Ru-Loaded Nanoparticles against U87 MG Cells. The cells were treated with increasing concentrations of Ru-loaded nanoparticles and incubated for 2 h. To remove the non-internalized nanoparticles, the medium was removed and fresh medium was added to the wells. Twenty-four or seventy-two hours later, the cell viability was evaluated (CCK-8). The reagent was directly mixed with fresh medium and placed in contact with the cells for 1 h at 37 °C. Then, the absorbance at 450 nm was read. The viability was plotted as a percentage (%) of the absorbance normalized for the controls.

Cytotoxicity of Ru-Loaded Nanoparticles against A2780 and CHO Cells. Either tumoral (A2780) or nontumoral ovarian cells (CHO) were seeded onto 96-well plates (5000 cells/well) and incubated overnight at 37 °C in a humidified incubator with 5% CO_2. Cells treated with Ru@MSN or Ru@A-MSN were added at the indicated concentrations for 72 h. Cell medium was removed by suction, and 50 μL of Thiazolyl Blue Tetrazolium Bromide (MTT, 1 mg/mL) was added to the wells following a 4 h incubation under the same experimental conditions. Then, the MTT solution was removed and pure DMSO (50 μL) was used to solubilize the formazan crystal formed in active cells. The absorbance was measured using a FLUOstar Omega microplate reader at λ = 570 nm. The experiment was perfomed in duplicate using six replicates. Data were analyzed with SigmaPlot 14.0 and are represented as the mean ± the standard deviation.

Determination of the Amount of Intracellular Ruthenium in U87 Cells. The U87 cells were seeded in T 25 cm^2 flasks at high density and properly cultured until 70−80% confluence was achieved. Cells were then treated with drug-loaded nanoparticles or the free ruthenium complex at the indicated concentrations for 12, 24, or 48 h. Cells were then trypsinized, collected, and counted using trypan blue staining. After centrifugation, cell pellets were digested using 30% Suprapur nitric acid for 24 h. The amount of metal element ruthenium was determined using inductively coupled plasma mass spectrometry (ICP-MS) in an Aligent Technologies system. Two independent measurements for each replicate were taken.

Cell Cycle Progression Analysis. Cell cycle analysis in U87 cells was evaluated by flow cytometry using propidium iodide staining. Briefly, 80000 cells/well were seeded onto 12-well plates and incubated overnight at 37 °C and 5% CO_2. Nanoparticles or cisplatin was added at the indicated concentrations for 24 h. Cells were then collected by trypsinization and fixed in a 7:3 EtOH/PBS solution for 4 h. After fixation, cells were centrifuged, washed with PBS, and stained with a propidium iodide (40 μg/mL) solution containing RNase (1 μg/mL) for 30 min. Cells were then subjected to flow cytometry (Beckmann Coulter Epics XL) registering fluorescence at 620 nm in the FL2-A channel. Two independent experiments were performed (n = 2 replicates), and data analyzed using Flowing Software 2.5.1.

Apoptosis Induction Assay. The impact of nanoparticles on the rate of apoptosis and necrosis in U87 cells was evaluated by flow cytometry using dual Annexin V/propidium iodide staining. Briefly, 80000 cells/well were seeded onto 12-well plates and incubated overnight at 37 °C in a humidified incubator with 5% CO_2. Either nanoparticles, the equitoxic free complex, or cisplatin was added at the indicated concentrations for 24 h. Cells were then collected by trypsinization, washed with binding buffer, and stained with an Annexin V-FLUOS/propidium iodide solution (eBioscience) as instructed by the manufacturer. Cells were then subjected to flow cytometry (Beckmann Coulter Epics XL) registering fluorescence at 530 and 620 nm in FL1-H and FL2-H, respectively. Two independent experiments were performed (n = 2 replicates), and data analyzed using Flowing Software 2.5.1.

■ ASSOCIATED CONTENT

Supporting Information

The Supporting Information is available free of charge at https://pubs.acs.org/doi/10.1021/acs.inorgchem.0c01436.

FTIR spectra, DLS measurements, TEM−EDX analysis, absorption spectra, release kinetics, and cell-based *in vitro* experiments (PDF)

■ AUTHOR INFORMATION

Corresponding Authors

Marina Martínez-Carmona − *School of Chemistry and CRANN, Trinity College, The University of Dublin (TCD), Dublin 2, Ireland;* orcid.org/0000-0002-2026-6266; Email: marinm11@ucm.es

José Ruiz − *Departamento de Química Inorgánica, Universidad de Murcia, and Biomedical Research Institute of Murcia (IMIB-Arrixaca), E-30071 Murcia, Spain;* orcid.org/0000-0002-0834-337X; Phone: +34 868887455; Email: jruiz@um.es

Maria Vallet-Regí − *Department of Chemistry in Pharmaceutical Sciences, School of Pharmacy, Universidad Complutense de Madrid, 28040 Madrid, Spain; Centro de Investigación Biomédica en Red de Bioingeniería, Biomateriales y Nanomedicina (CIBER-BBN), 28029 Madrid, Spain;* Phone: +34 91 394 1843; Email: vallet@ucm.es

Authors

Qui P. Ho − *School of Pharmacy and Pharmaceutical Sciences, Trinity College Dublin (TCD), Dublin 2, Ireland; Trinity Biomedical Sciences Institute, TCD, Dublin 2, Ireland*

Jérémy Morand − *School of Chemistry and CRANN, Trinity College, The University of Dublin (TCD), Dublin 2, Ireland*

Ana García − *Department of Chemistry in Pharmaceutical Sciences, School of Pharmacy, Universidad Complutense de Madrid, 28040 Madrid, Spain; Centro de Investigación Biomédica en Red de Bioingeniería, Biomateriales y Nanomedicina (CIBER-BBN), 28029 Madrid, Spain*

Enrique Ortega − *Departamento de Química Inorgánica, Universidad de Murcia, and Biomedical Research Institute of Murcia (IMIB-Arrixaca), E-30071 Murcia, Spain*

Luiza C. S. Erthal − *School of Pharmacy and Pharmaceutical Sciences, Trinity College Dublin (TCD), Dublin 2, Ireland; Trinity Biomedical Sciences Institute, TCD, Dublin 2, Ireland*

Eduardo Ruiz-Hernandez − *School of Pharmacy and Pharmaceutical Sciences, Trinity College Dublin (TCD), Dublin 2, Ireland; Trinity Biomedical Sciences Institute, TCD, Dublin 2, Ireland*

M. Dolores Santana − *Departamento de Química Inorgánica, Universidad de Murcia, and Biomedical Research Institute of Murcia (IMIB-Arrixaca), E-30071 Murcia, Spain;* orcid.org/0000-0002-1446-8232

Yurii Gun'ko − *School of Chemistry and CRANN, Trinity College, The University of Dublin (TCD), Dublin 2, Ireland;* orcid.org/0000-0002-4772-778X

Complete contact information is available at: https://pubs.acs.org/10.1021/acs.inorgchem.0c01436

Notes

The authors declare no competing financial interest.

■ ACKNOWLEDGMENTS

M.M.-C. thanks the Irish Research Council (postdoctoral fellowship) for the financial support. The European Research

Council, ERC-2015-AdG (VERDI), Proposal 694160; Ministerio de Ciencia, Innovación y Universidades, Fundación Séneca-CARM (Project 20857/PI/18); and FEDER funds (Grant RTI2018-096891-B-I00 and MultiMetDrugs network RED2018-102471-T) also supported this work. E.O. thanks AECC (Project 20277/FPI/17). E.R.-H. is grateful to the Wellcome Trust Institutional Strategic Support Fund and the European Research Council (Grant Agreement 758887).

REFERENCES

(1) World Health Organizaton. Cancer. https://www.who.int/health-topics/cancer.
(2) McNeill, K. A. Epidemiology of Brain Tumors. *Neurologic Clinics* **2016**, *34* (4), 981−998.
(3) Bush, N. A. O.; Chang, S. M.; Berger, M. S. Current and Future Strategies for Treatment of Glioma. *Neurosurg Rev.* **2017**, *40* (1), 1−14.
(4) *Cancer Facts & Figures 2020*; American Cancer Society: Atlanta, 2020; pp 1−76.
(5) Fan, W.; Yung, B.; Huang, P.; Chen, X. Nanotechnology for Multimodal Synergistic Cancer Therapy. *Chem. Rev.* **2017**, *117* (22), 13566−13638.
(6) Zeng, L.; Gupta, P.; Chen, Y.; Wang, E.; Ji, L.; Chao, H.; Chen, Z.-S. The Development of Anticancer Ruthenium(II) Complexes: From Single Molecule Compounds to Nanomaterials. *Chem. Soc. Rev.* **2017**, *46* (19), 5771−5804.
(7) Meier-Menches, S. M.; Gerner, C.; Berger, W.; Hartinger, C. G.; Keppler, B. K. Structure-Activity Relationships for Ruthenium and Osmium Anticancer Agents - towards Clinical Development. *Chem. Soc. Rev.* **2018**, *47* (3), 909−928.
(8) Yan, Y. K.; Melchart, M.; Habtemariam, A.; Sadler, P. J. Organometallic Chemistry, Biology and Medicine: Ruthenium Arene Anticancer Complexes. *Chem. Commun.* **2005**, No. 38, 4764.
(9) Wachter, E.; Zamora, A.; Heidary, D. K.; Ruiz, J.; Glazer, E. C. Geometry Matters: Inverse Cytotoxic Relationship for Cis/Trans-Ru(II) Polypyridyl Complexes from Cis/Trans-$[PtCl_2(NH_3)_2]$. *Chem. Commun.* **2016**, *52* (66), 10121−10124.
(10) Bergamo, A.; Sava, G. Linking the Future of Anticancer Metal-Complexes to the Therapy of Tumour Metastases. *Chem. Soc. Rev.* **2015**, *44* (24), 8818−8835.
(11) Trondl, R.; Heffeter, P.; Kowol, C. R.; Jakupec, M. A.; Berger, W.; Keppler, B. K. NKP-1339, the First Ruthenium-Based Anticancer Drug on the Edge to Clinical Application. *Chem. Sci.* **2014**, *5* (8), 2925−2932.
(12) Noffke, A. L.; Habtemariam, A.; Pizarro, A. M.; Sadler, P. J. Designing Organometallic Compounds for Catalysis and Therapy. *Chem. Commun.* **2012**, *48* (43), 5219−5246.
(13) Hartinger, C. G.; Metzler-Nolte, N.; Dyson, P. J. Challenges and Opportunities in the Development of Organometallic Anticancer Drugs. *Organometallics* **2012**, *31* (16), 5677−5685.
(14) Murray, B. S.; Babak, M. V.; Hartinger, C. G.; Dyson, P. J. The Development of RAPTA Compounds for the Treatment of Tumors. *Coord. Chem. Rev.* **2016**, *306*, 86−114.
(15) Yellol, G. S.; Donaire, A.; Yellol, J. G.; Vasylyeva, V.; Janiak, C.; Ruiz, J. On the Antitumor Properties of Novel Cyclometalated Benzimidazole Ru(II), Ir(III) and Rh(III) Complexes. *Chem. Commun.* **2013**, *49* (98), 11533−11535.
(16) Shen, J.; Kim, H.-C.; Wolfram, J.; Mu, C.; Zhang, W.; Liu, H.; Xie, Y.; Mai, J.; Zhang, H.; Li, Z.; Guevara, M.; Mao, Z.-W.; Shen, H. A Liposome Encapsulated Ruthenium Polypyridine Complex as a Theranostic Platform for Triple-Negative Breast Cancer. *Nano Lett.* **2017**, *17* (5), 2913−2920.
(17) Zhang, P.; Wang, J.; Huang, H.; Yu, B.; Qiu, K.; Huang, J.; Wang, S.; Jiang, L.; Gasser, G.; Ji, L.; Chao, H. Unexpected High Photothemal Conversion Efficiency of Gold Nanospheres upon Grafting with Two-Photon Luminescent Ruthenium(II) Complexes: A Way towards Cancer Therapy? *Biomaterials* **2015**, *63*, 102−114.
(18) Yang, G.-G.; Hao, L.; Cao, Q.; Zhang, H.; Yang, J.; Ji, L.-N.; Mao, Z.-W. Three-in-One Self-Assembled Nanocarrier for Dual-Drug Delivery, Two-Photon Imaging, and Chemo-Photodynamic Synergistic Therapy. *ACS Appl. Mater. Interfaces* **2018**, *10* (34), 28301−28313.
(19) He, L.; Huang, Y.; Zhu, H.; Pang, G.; Zheng, W.; Wong, Y.-S.; Chen, T. Cancer-Targeted Monodisperse Mesoporous Silica Nanoparticles as Carrier of Ruthenium Polypyridyl Complexes to Enhance Theranostic Effects. *Adv. Funct. Mater.* **2014**, *24* (19), 2754−2763.
(20) Ellahioui, Y.; Patra, M.; Mari, C.; Kaabi, R.; Karges, J.; Gasser, G.; Gómez-Ruiz, S. Mesoporous Silica Nanoparticles Functionalised with a Photoactive Ruthenium(II) Complex: Exploring the Formulation of a Metal-Based Photodynamic Therapy Photosensitiser. *Dalton Transactions* **2019**, *48* (18), 5940−5951.
(21) Martínez-Carmona, M.; Colilla, M.; Vallet-Regí, M. Smart Mesoporous Nanomaterials for Antitumor Therapy. *Nanomaterials* **2015**, *5* (4), 1906−1937.
(22) Martínez-Carmona, M.; Gun'ko, Y. K.; Vallet-Regí, M. Mesoporous Silica Materials as Drug Delivery: "The Nightmare" of Bacterial Infection. *Pharmaceutics* **2018**, *10* (4), 279.
(23) Baeza, A.; Colilla, M.; Vallet-Regí, M. Advances in Mesoporous Silica Nanoparticles for Targeted Stimuli-Responsive Drug Delivery. *Expert Opin. Drug Delivery* **2015**, *12* (2), 319−337.
(24) Shen, S.-C.; Ng, W.; Onn Chia, L.; Dong, Y.-C.; Hee Tan, R. Applications of Mesoporous Materials as Excipients for Innovative Drug Delivery and Formulation. *Curr. Pharm. Des.* **2013**, *19* (35), 6270−6289.
(25) Sun, T.; Zhang, Y. S.; Pang, B.; Hyun, D. C.; Yang, M.; Xia, Y. Engineered Nanoparticles for Drug Delivery in Cancer Therapy. *Angew. Chem., Int. Ed.* **2014**, *53* (46), 12320−12364.
(26) Raza, A.; Rasheed, T.; Nabeel, F.; Hayat, U.; Bilal, M.; Iqbal, H. M. N. Endogenous and Exogenous Stimuli-Responsive Drug Delivery Systems for Programmed Site-Specific Release. *Molecules* **2019**, *24* (6), 1117.
(27) Martínez-Carmona, M.; Lozano, D.; Colilla, M.; Vallet-Regí, M. Lectin-Conjugated PH-Responsive Mesoporous Silica Nanoparticles for Targeted Bone Cancer Treatment. *Acta Biomater.* **2018**, *65*, 393−404.
(28) Santha Moorthy, M.; Bharathiraja, S.; Manivasagan, P.; Lee, K. D.; Oh, J. Synthesis of Surface Capped Mesoporous Silica Nanoparticles for PH-Stimuli Responsive Drug Delivery Applications. *MedChemComm* **2017**, *8* (9), 1797−1805.
(29) Martínez-Carmona, M.; Lozano, D.; Colilla, M.; Vallet-Regí, M. Selective Topotecan Delivery to Cancer Cells by Targeted PH-Sensitive Mesoporous Silica Nanoparticles. *RSC Adv.* **2016**, *6* (56), 50923−50932.
(30) Duo, Y.; Li, Y.; Chen, C.; Liu, B.; Wang, X.; Zeng, X.; Chen, H. DOX-Loaded PH-Sensitive Mesoporous Silica Nanoparticles Coated with PDA and PEG Induce pro-Death Autophagy in Breast Cancer. *RSC Adv.* **2017**, *7* (63), 39641−39650.
(31) Wen, J.; Yan, H.; Xia, P.; Xu, Y.; Li, H.; Sun, S. Mesoporous Silica Nanoparticles-Assisted Ruthenium(II) Complexes for Live Cell Staining. *Sci. China: Chem.* **2017**, *60* (6), 799−805.
(32) Wencel, D.; Dolan, C.; Barczak, M.; Keyes, T. E.; McDonagh, C. Synthesis, Tailoring and Characterization of Silica Nanoparticles Containing a Highly Stable Ruthenium Complex. *Nanotechnology* **2013**, *24* (36), 365705.
(33) Frasconi, M.; Liu, Z.; Lei, J.; Wu, Y.; Strekalova, E.; Malin, D.; Ambrogio, M. W.; Chen, X.; Botros, Y. Y.; Cryns, V. L.; Sauvage, J.-P.; Stoddart, J. F. Photoexpulsion of Surface-Grafted Ruthenium Complexes and Subsequent Release of Cytotoxic Cargos to Cancer Cells from Mesoporous Silica Nanoparticles. *J. Am. Chem. Soc.* **2013**, *135* (31), 11603−11613.
(34) Lv, G.; Qiu, L.; Liu, G.; Wang, W.; Li, K.; Zhao, X.; Lin, J. PH Sensitive Chitosan-Mesoporous Silica Nanoparticles for Targeted Delivery of a Ruthenium Complex with Enhanced Anticancer Effects. *Dalton Transactions* **2016**, *45* (45), 18147−18155.
(35) Novohradsky, V.; Yellol, J.; Stuchlikova, O.; Santana, M. D.; Kostrhunova, H.; Yellol, G.; Kasparkova, J.; Bautista, D.; Ruiz, J.;

https://dx.doi.org/10.1021/acs.inorgchem.0c01436
Inorg. Chem. XXXX, XXX, XXX−XXX

804 Brabec, V. Organoruthenium Complexes with ĈN Ligands Are Highly
805 Potent Cytotoxic Agents That Act by a New Mechanism of Action.
806 *Chem. - Eur. J.* **2017**, *23* (61), 15294−15299.
807 (36) Haul, R. S. J.; Gregg, K. S. W. Sing: Adsorption, Surface Area
808 and Porosity. 2. Auflage, Academic Press, London 1982. 303 Seiten,
809 Preis: $ 49.50. *Berichte der Bunsengesellschaft für physikalische Chemie*
810 **1982**, *86* (10), 957−957.
811 (37) Balas, F.; Manzano, M.; Colilla, M.; Vallet-Regí, M. L -Trp
812 Adsorption into Silica Mesoporous Materials to Promote Bone
813 Formation. *Acta Biomater.* **2008**, *4*, 514−522.
814 (38) Cho, E. C.; Xie, J.; Wurm, P. A.; Xia, Y. Understanding the Role
815 of Surface Charges in Cellular Adsorption versus Internalization by
816 Selectively Removing Gold Nanoparticles on the Cell Surface with a I
817 2 /KI Etchant. *Nano Lett.* **2009**, *9* (3), 1080−1084.
818 (39) Paris, J. L.; de la Torre, P.; Manzano, M.; Cabañas, M. V.;
819 Flores, A. I.; Vallet-Regí, M. Decidua-Derived Mesenchymal Stem
820 Cells as Carriers of Mesoporous Silica Nanoparticles. In Vitro and in
821 Vivo Evaluation on Mammary Tumors. *Acta Biomater.* **2016**, *33*,
822 275−282.
823 (40) Ormerod, M. G.; Orr, R. M.; Peacock, J. H. The Role of
824 Apoptosis in Cell Killing by Cisplatin: A Flow Cytometric Study. *Br. J.*
825 *Cancer* **1994**, *69* (1), 93−100.
826 (41) Martínez-Carmona, M.; Izquierdo-Barba, I.; Colilla, M.; Vallet-
827 Regí, M. Concanavalin A-Targeted Mesoporous Silica Nanoparticles
828 for Infection Treatment. *Acta Biomater.* **2019**, *96*, 547−556.

https://dx.doi.org/10.1021/acs.inorgchem.0c01436
Inorg. Chem. XXXX, XXX, XXX−XXX